Journal of Optoelectronics and Advanced Materials, Vol. 2, No. 1, March 2000, p. 73-81

INNOVATIVE TELESCOPE FOR 3-D LIDAR MEASUREMENTS

A. Amodeo[a], A. Boselli[a], L. Fiorani[b], G. Passeggio[c], R. Velotta[d]

[a]Istituto di Metodologie Avanzate di Analisi Ambientale, Consiglio Nazionale delle Ricerche, Area della Ricerca di Potenza, C.da S. Loja, I-85050 Tito Scalo (PZ), Italy
[b]CORISTA, P.le Tecchio 80, I-80125 Napoli, Italy
[c]INFN, Sezione di Napoli, Dipartimento di Scienze Fisiche, Complesso Universitario di Monte S. Angelo, Via Cintia, I-85126 Napoli, Italy
[d]INFM, Unità di Napoli, Dipartimento di Scienze Fisiche, Complesso Universitario di Monte S. Angelo, Via Cintia, I-85126 Napoli, Italy

Lidar has been used since the sixties to measure atmospheric parameters and air pollution. In order to allow its routine employment in field campaigns, we have developed a system based on an innovative telescope: with respect to other instruments, the one presented here is inexpensive, compact, easy to adjust, provided with a remarkable depth of field and can be aimed to any direction avoiding transmitter-receiver misalignment. Its development has required a remarkable effort in the design and realization of state-of-the-art mechanical parts. The first data acquisitions demonstrate its good optical performances in spite of the relatively small diameter of the primary mirror.

(Received November 17, 1999; accepted after revision February 2, 2000)

Keywords: Lidar, Optics, Precision mechanics

1. Introduction

Air pollution [1] is one of the most important problems of our planet. Range- and time-resolved measurements of atmospheric parameters are necessary to understand the physico-chemical processes that determine the air quality. "In situ" sensors [2] have been developed earlier and are routinely used to monitor the air quality in our towns. Remote sensors, such as lidars [3, 4], spread in the last decades thanks to their unrivalled advantages with respect to the current techniques. First of all, remote sensors are probeless: this implies that the possibility of modifying the air sample is eliminated. Secondly, their measurements are accomplished along a path, thus avoiding biases linked to local effects. Finally, they are able to retrieve the profile of atmospheric parameters over a considerable range and with good spatial and temporal resolution. Besides those advantages, generally common to remote sensors, in principle lidar could sweep the complete hemisphere. In this way, the physico-chemical parameters of an air parcel can be continuously monitored, providing atmospheric modelers with valuable information.

Even if lidar has demonstrated to be a powerful technique, its utilization in field campaigns requires a careful system design, especially if one wants to keep the above-mentioned capability of sweeping in a compact instrument. This paper describes one of the three identical telescopes developed in the framework of the INFM program "Progetto Sud – Tecniche ottiche innovative per il monitoraggio ambientale e piani di tutela e risanamento" supported by the European Fund for Regional Development.

2. Lidar

A lidar is an optical radar: usually the transmitter is a laser and the receiver a telescope. The lidar equation [4] can be written as follows:

$$P(R) = k\xi(R)P_0 \frac{A}{R^2}\beta(R)\frac{c\tau}{2}exp\left[-2\int_0^R \alpha(R')dR'\right], \quad (1)$$

where P is the detected power, R is the range, k is a constant taking into account the detection efficiency, ξ is the overlap function between the telescope field of view (FOV) and the laser beam, P_0 is the emitted power, A is the telescope area, β is the atmospheric backscattering coefficient, c is the speed of light, τ is the duration of the laser pulse and α is the atmospheric extinction coefficient. The physicochemical parameters of the atmosphere along the laser beam are inferred from the optical properties of the corresponding air parcel (α and β). R depends on t, the time interval between emission and detection, as $R=ct/2$ [4].

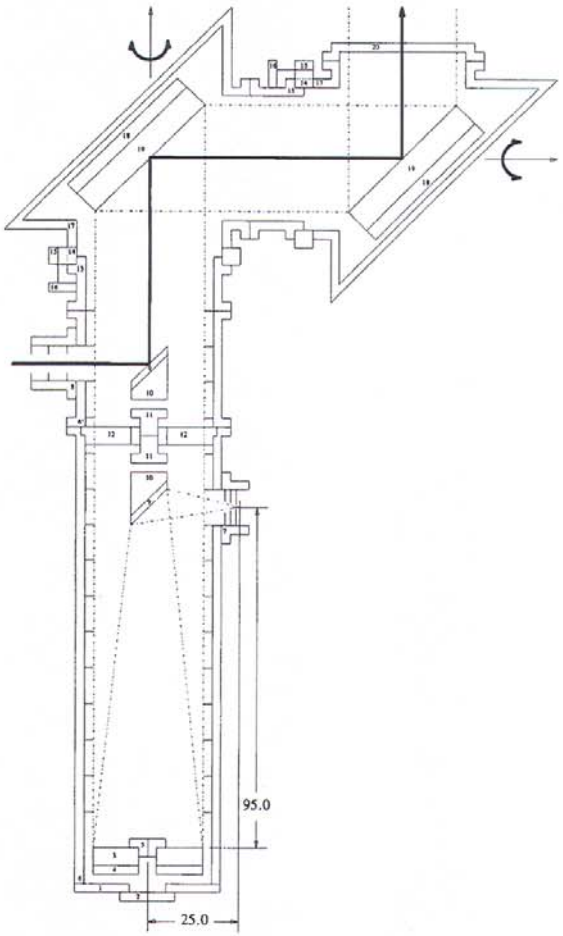

Fig. 1. Scheme of the telescope. 1: breech; 2: lid; 3: round mirror (diameter: 30.5 cm, thickness: 5 cm); 4: mirror mount; 5: iris diaphragm; 6 and 6': tubes (inner diameter: 35 cm) with equidistant baffles (inner diameter: 31 cm); 7: connection with detector (with baffles); 8: connection with laser (with baffles); 9: elliptical mirror (major axis: 10 cm, minor axis: 7 cm, thickness: 2 cm); 10: mirror mount; 11: holder; 12: spider blade; 13: tube; 14: gear wheel; 15: pinion; 16: stepper motor; 17: mirror housing; 18: mirror mount; 19: octagonal mirror (major axis: 46.5 cm, minor axis: 33 cm; thickness: 5 cm); 20: lid.

3. Telescope design

The lidar under development for the above-mentioned INFM program was aimed to the three-dimensional mapping of pollutants in the planetary boundary layer (low troposphere). The feasibility study, based on a simulation of the measurement and a ray tracing analysis [5], showed that a telescope diameter of 30 cm is adequate for this purpose. Taking into account such result, the following design choices were made:

- monostatic configuration (transmitter and receiver on the same axis), to make easier the transmitter-receiver alignment;
- Newton telescope with short focal length, to bring nearer the overlap between the telescope FOV and the laser beam;
- coelostat (system of two scanning mirrors) to sweep the complete hemisphere, avoiding transmitter-receiver misalignment.

The scheme of the telescope is given in Fig. 1. The laser beam (solid thick line) hits the upper elliptical mirror and the octagonal mirrors able to rotate around the axes indicated by the arrows: in this way it can be turned in any direction. The light backscattered by the atmosphere (dashed line) is gathered by the two octagonal mirrors, the round mirror (Newton primary) and the lower elliptical mirror (Newton secondary), before reaching the detector. As regards the scanning mirrors, the octagon has been preferred to the ellipse because of the considerable money saving, even if it is slightly larger (the ellipse is inscribed in the octagon).

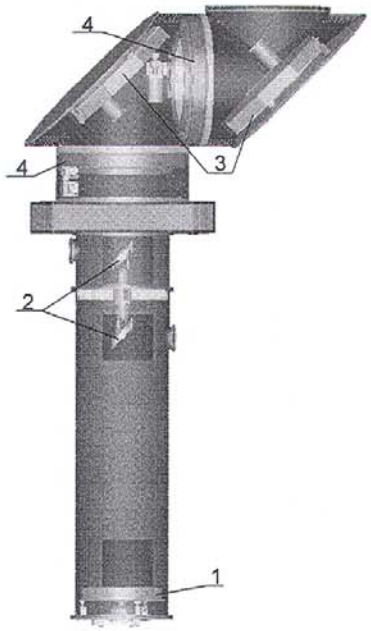

Fig. 2. Picture of the telescope. 1: round mirror; 2: elliptical mirror; 3: octagonal mirror; 4: rotary actuator.

In order to operate properly, each component of the telescope has to be precisely aligned (within about 1 mrad). Such requirement has been met thanks to a careful design of the mechanical parts. Some pictures of the final system and of the key particulars are given in Fig. 2 and 3, respectively.

Let us now describe in more detail such key particulars: round mirror mount, elliptical mirror mount, octagonal mirror mount, rotary actuator.

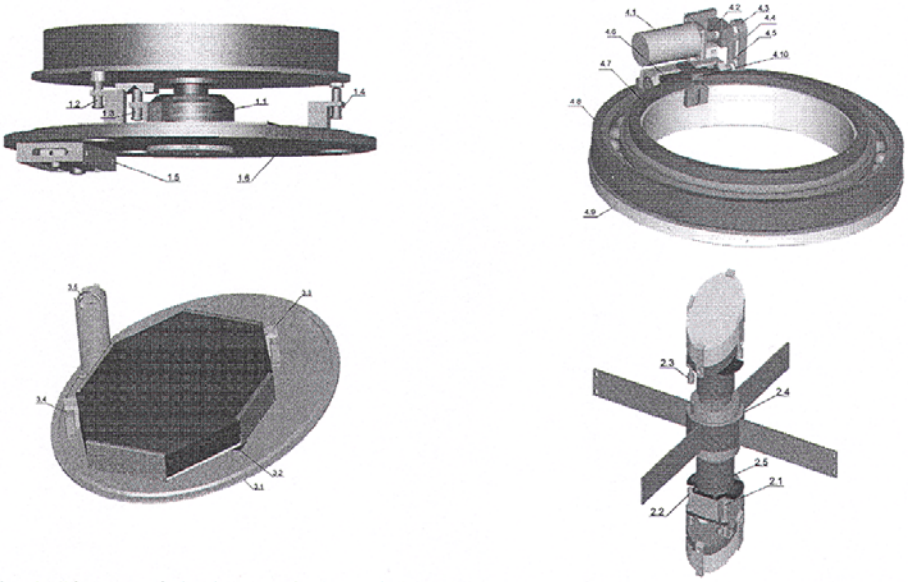

Fig. 3. Pictures of the key particulars of the telescope. Round mirror mount. 1.1: spring; 1.2-5: fine adjustment screws; 1.6 : screws.Elliptical mirror mount. 2.1-3: fine adjustment screws; 2.4: holder; 2.5 barrel. Octagonal mirror mount. 3.1: flange; 3.2-4: fine adjustment screws; 3.5: spring. Rotary actuator. 4.1: stepper motor; 4.2: joint; 4.3: gear wheel; 4.4: timing belt 4.5: gear wheel; 4.6: tangent screw; 4.7: gear wheel; 4.8-9: flange; 4.10: switch.

The tilt of the round mirror is controlled by three fine adjustment screws and one resisting spring. The screws have a 0.75-mm pitch thread. The distance of any screw from the corresponding rotation axis is 210 mm. Taking into account these data and assuming a minimum screw rotation of 1/16 of turn, the minimum tilt is 0.22 mrad. To center the round mirror with respect to the optical axis, the screws 1.6 (see Fig. 3) have to be loosened and the fine adjustments have to be performed by screws 1.5. In this way, an accuracy of about 0.01 mm can be reached in the round mirror centering with respect to the optical axis.

The barrel 2.5 can be screwed in the holder 2.4 (see Fig. 3): in this way, the elliptical mirror can be turned to the corresponding opening and translated along the optical axis (pitch: 1 mm, stroke: 20 mm). The minimum tilt is 0.26 mrad (pitch thread: 0.2 mm, distance: 48 mm). Acting simultaneously on the three screws, a minimum translation of about 0.01 mm can be obtained. The mirror mount design has been carefully aimed to the minimum light loss: actually, the mount involves a 0.6% loss, negligible with respect to the overall obstruction (~6%) due to elliptical mirrors.

The assembly of the octagonal mirror mount takes into account the weight of the mirror (18 kg) and the vibrations involved in the coelostat movements. The minimum tilts corresponding to screws 3.3 (pitch thread: 0.75 mm, distance: 435 mm) and 3.4 (pitch thread: 0.75 mm, distance: 305 mm) are, respectively, 0.11 and 0.15 mrad.

The stepper motor (200 steps per revolution) fits the gear wheel 4.3 by means of the joint (see Fig. 3). The motor rotation is transferred to the gear wheel 4.7 via the timing belt, the gear wheel 4.5 and the tangent screw: the velocity ratio is 1:253. The minimum angle between the flanges 4.8 and 4.9 that one can obtain operating the motor is 0.12 mrad. The design of the rotary actuator ensures an angle accuracy of about 10 mrad and a speed of 2 revolutions per minute. A switch assigns the point of reference to the software controlling the motor.

The angle accuracy of the rotary actuator is very good, taking into account that realistic sweeps of the hemisphere will involve angle steps of at least around 100 mrad. The minimum tilt of the mirror mounts is well below what is necessary for an accurate alignment (about 1 mrad).

The feasibility study of the optics and the design of the mechanical parts allowed us not only to develop a sweeping telescope with good angle accuracy and minimum tilt, but also to reach a set of performances that are not contemporarily present in similar instruments. First of all, the system

presented here is less expensive of about a factor 3. Secondly, it is remarkably compact: its overall volume does not exceed 0.8 m^3. Moreover, it is easy to adjust: the correct overlap between the telescope FOV and the laser beam can be obtained within few minutes of operation. In addition, its remarkable depth of field allows the researchers to probe the lower atmospheric layers. Finally, it can be aimed to any direction avoiding transmitter-receiver misalignment thanks to the coelostat, because its flat mirrors preserve the correct overlap between the telescope FOV and the laser beam once it has been obtained for one given direction.

4. System alignment and control

The telescope alignment is performed according to the following procedure (see Fig. 4). First, the telescope axis is defined by using a semiconductor laser beam, mounted before the primary mirror, and a flat mirror, placed on the opposite side so that the laser beam is reflected along the same path (Fig. 4a). Successively, the secondary mirror is mounted and oriented in such a way that the same laser beam is reflected across the center of the telescope exit aperture (Fig. 4b). Then, the focal plane of the telescope is found. This is achieved by measuring the distance, from the telescope exit, at which the image of a diffuse light source, placed at the telescope exit, is produced. Finally, this image is centered across the telescope exit aperture by tilting the primary mirror (Fig. 4c).

The alignment of the octagonal mirrors of the coelostat is accomplished by following an iterative procedure:

1) a target at a distance much greater than the linear dimension of the coelostat is aimed;
2) both the octagonal mirrors are rotated by 180°;
3) the tilting screws of the mirrors are then adjusted in order to aim the same target of the first step;
4) the two mirrors are rotate back in the original position and the alignment is obtained by repeating the procedure.

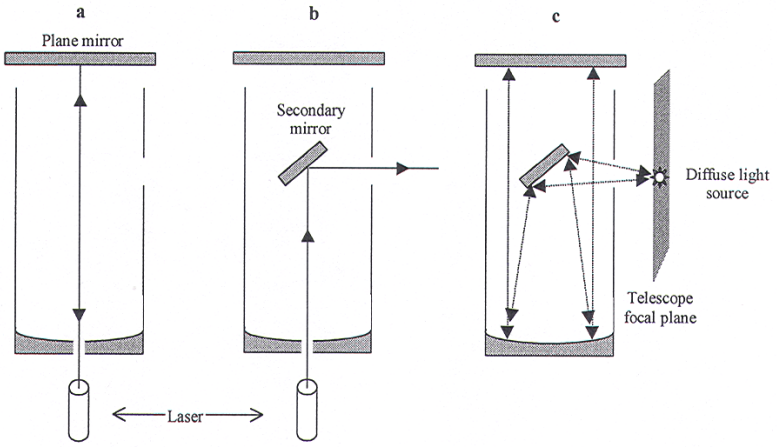

Fig. 4. Scheme of the telescope alignment procedure.

The movement of the octagonal mirrors is performed by two motor drivers controlled by a single device. Movement speed, direction and commands are sent to the controller through a RS232 serial line from a PC (see Fig. 5).

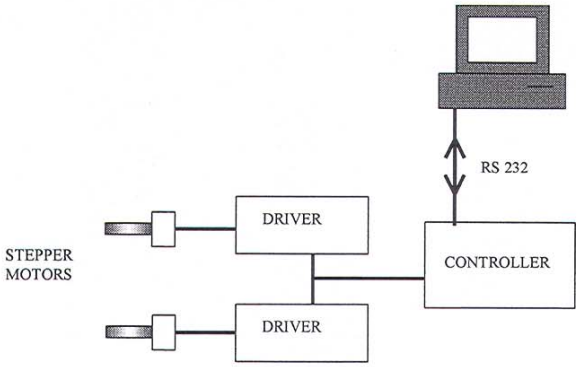

Fig. 5. Scheme of the electronics controlling the stepper motors.

5. Data acquisition

In this section we report on two examples of data acquisition performed in different experimental conditions. As a first example, Fig. 6 shows the lidar echoes from a stack emission plume registered during a field measurements campaign in an industrial area of Southern Italy (S. Nicola di Melfi).

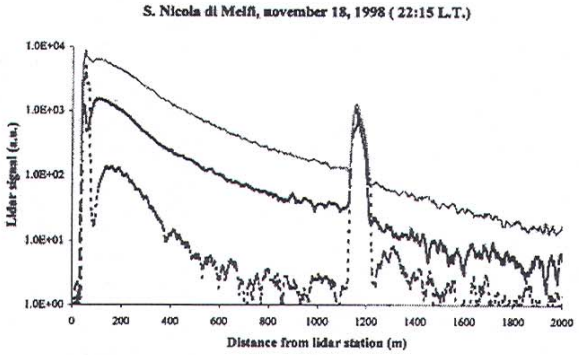

Fig. 6. Lidar echoes from a stack emission plume at three different laser wavelengths (solid gray line: 355 nm; solid black line: 532 nm; dashed black line: 1064 nm).

The transmitter was based on a Nd:YAG laser delivering simultaneously the fundamental (1064 nm), the second (532 nm) and third (355 nm) harmonics, with a maximum repetition rate of 20 Hz. The receiver included a system of spectral selection based on dichroic mirrors and interference filters. The data were acquired by photomultiplier tubes and photon counting chains for each channel (see Table 1 for system specifications). The measurements of the stack emission plume have been performed at three different wavelengths simultaneously (355 nm, 532 nm and 1064 nm). Each profile has been retrieved averaging 3000 laser shots and has a spatial resolution of 3 m. The optical depth and the integrated backscattering coefficient of the plume have been evaluated showing that sub-micrometric particles are emitted from the stack [6]. Another interest of the data acquisition presented here is the first application to lidar measurements, to the best of our knowledge, of a recently developed infrared photomultiplier tube.

Table 1. Specifications of the lidar used for the data acquisition of Fig. 6.

Element	Parameter	Value
laser	maximum pulse energy at 1064 nm	600 mJ
	maximum pulse energy at 532 nm	300 mJ
	maximum pulse energy at 355 nm	180 mJ
	maximum pulse repetition rate	20 Hz
	pulse duration	5 – 7 ns
	beam divergence	< 0.5 mrad
dichroic mirrors	reflectivity (selected harmonic)	> 99%
	reflectivity (other harmonics)	< 10%
interference filters	bandwidth	~ 1 nm
	transmission	~ 20 %
	out of band rejection	10^{-8}
photomultiplier (1064 nm)	quantum efficiency	~ 0.08 %
	gain	2×10^5
photomultipliers (532 and 355 nm)	quantum efficiency	~ 22 %
	gain	8×10^5
counting chains	minimum threshold	10 mV
	maximum time resolution	5 ns
	maximum input rate	150 MHz
	maximum count per channel	1 (dwell time = 5 ns) 15 (20 ns < dwell time < 70 ns) 10^6 (dwell time > 70 ns)

A further example of lidar profile is given in Fig. 7. The data acquisition (1000 laser shots) was performed at the University of Lecce. The transmitter was based on a KrF excimer laser (wavelength: 248 nm, energy per pulse: 60 mJ, repetition rate: 10 Hz). The receiver included a spectrometer and a photomultiplier tube whose signal was observed by a digital oscilloscope (see Table 2 for system specifications). In order to make more readable the plot, in Fig. 7 we show the range corrected signal (RCS) i.e. the logarithm of the product of the signal times the square of the range.

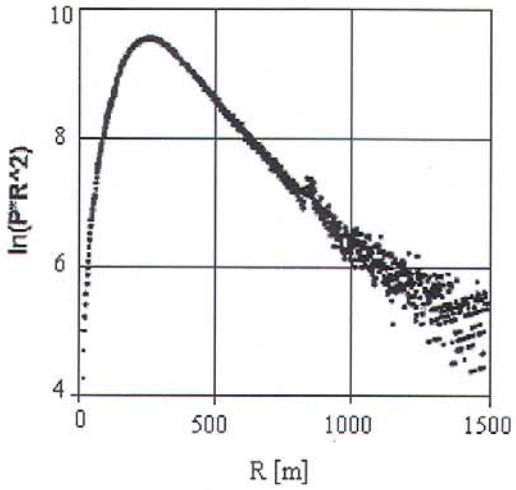

Fig. 7. Range corrected signal as a function of height (Lecce, september 9, 1998)

The overlap between the telescope FOV and the laser beam completes at 250 m (increase of the RCS). Between 250 and 800 m the atmosphere seems to have constant optical properties (linear decrease of the RCS), corresponding to a homogeneous air layer. At 800 m the RCS presents a peak, probably due to a thin aerosol layer (high backscattering coefficient). After the attenuation arisen from the aerosol, the signal to noise ratio deteriorates rapidly and the fluctuation dominates at around 1500 m.

Table 2. Specifications of the lidar used for the data acquisition of Fig. 7.

Element	Parameter	Value
laser	pulse energy	60 mJ
	pulse repetition rate	10 Hz
	pulse duration	20 ns
	beam divergence	1 mrad
spectrometer	bandwidth	4 nm
	transmission	30 %
	out of band rejection	10^{-6}
photomultiplier	quantum efficiency	~ 20 %
	gain	~ 10^{6}
oscilloscope	dynamic range	8 bit
	conversion rate	100 MHz

With respect to other telescopes used by the authors, the innovative one presented here showed good optical performances in spite of the relatively small diameter of the primary mirror (see the clear identification of the stack emission plume more than 1 km away in Fig. 6). Moreover, the transmitter-receiver alignment was very easy taking only few minutes during the first operation. Finally, the

system has the unique capability of sweeping the complete hemisphere: this made possible, for instance, to aim the stack emission plume.

6. Conclusions

An innovative telescope for 3-D lidar measurements in the troposphere has been designed and realized in the framework of the INFM program "Progetto Sud – Tecniche ottiche innovative per il monitoraggio ambientale e piani di tutela e risanamento". After discussion of the main design choices, the positioning precision of the key components and alignment procedure of the system have been described. Finally, some examples of lidar profiles have been shown.

Acknowledgements

This study has been realized with the contribution of the INFM (Italian Institute for Matter Physics) and partially supported by the European Union. L. Fiorani is grateful to M. R. Perrone for the use of her laboratory facilities on the occasion of the data acquisition performed at the University of Lecce.

References

[1] J. B. Finlayson-Pitts, J. N. Pitts Jr., Atmospheric Chemistry, Wiley, New York, 1986.
[2] Air Pollution - Volume III: Measuring, Monitoring and Surveillance of Air Pollution, Ed. A. C. Stern, Academic Press, New York, 1977.
[3] L. Fiorani, J. of Optoelectronics and Advanced Materials, **1**(3), 3 (1999).
[4] R. M. Measures, Laser Remote Sensing, Krieger, Malabar, 1992.
[5] R. Velotta, B. Bartoli, R. Capobianco, L. Fiorani, N. Spinelli, Appl. Opt., **37**(30), 6999 (1998).
[6] P. F. Ambrico, A. Amodeo, S. Amoruso, M. Armenante, A. Boselli, M. Pandolfi, G. Pappalardo, N Spinelli, R. Velotta, Monitoring of an industrial area in Southern Italy by using a multi - wavelength lidar, Optica Applicata, **29**(4), 425 (1999).